JACS
JOURNAL OF THE AMERICAN CHEMICAL SOCIETY
pubs.acs.org/JACS
Article

Isoreticular Curves: A Theory of Capillary Condensation To Model Water Sorption within Microporous Sorbents

Julius J. Oppenheim and Mircea Dincă*

Cite This: J. Am. Chem. Soc. 2024, 146, 20615−20626
Read Online
ACCESS | Metrics & More | Article Recommendations | Supporting Information

ABSTRACT: Metal−organic frameworks have gained traction as leading materials for water sorption applications due to precise chemical tunability of their well-ordered pores. These applications include atmospheric water capture, heat pumps, desiccation, desalination, humidity control, and thermal batteries. However, the relationships between the framework pore structure and the measurable water sorption properties, namely critical relative humidity for condensation, maximal capacity, and pore size or temperature for the onset of hysteresis, have not been clearly delineated. Herein, we precisely formulate these relationships by application of the theory of capillary condensation and macroscopic thermodynamic models to a large data set of MOF water isotherms. These relationships include a concept termed *isoreticular curves* that relates the critical pressure for pore condensation (α), gravimetric capacity (Q_{max}), and hydrophilicity (the Gibbs free energy for binding water, ΔG) as $Q_{max} = a_1(\Delta G/\ln \alpha)^2 + a_2(\Delta G/\ln \alpha)$, with constants a_1 and a_2 dependent upon the density and volume occupied by the linker and secondary building unit, and framework topology. Through this analysis, we propose guidelines for the maximization of sorption capacity at a given relative humidity with minimal hysteresis and discuss the theoretical limits for capacity at low relative humidity. This model provides an explanation for the lack of high-capacity frameworks at low relative humidity, as increasing pore size also causes an increase in relative humidity. We propose a loose upper bound of $Q_{max} = -0.25(1/\ln \alpha)^2 - 1.75(1/\ln \alpha)$ for the limit of maximal capacity at a given relative humidity in the dry regime. These guidelines are consequential for the design of new materials for water sorption applications.

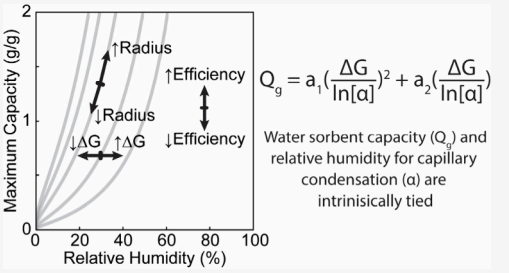

INTRODUCTION

Ideal sorbents for water sorption applications must be optimized with respect to several variables, including the relative humidity (RH) for capillary condensation, the maximum gravimetric capacity, the presence of hysteretic loops and their width, the cycling stability, the kinetics of cycling, the heat of adsorption, the cost of the material, and the environment and health impact of the material constituents.[1] Even though some of these parameters may be correlated,[2,3] the full multivariate optimization has proved to be fundamentally challenging. To date, no satisfactory theory that enables this optimization has been proposed. Herein, we discuss such a comprehensive theory that includes the RH for onset of capillary condensation, the maximum gravimetric capacity, and the presence of hysteretic loops. This theory will also be used to discuss the heat of adsorption and use of characteristic curves.

Of the materials for water sorption applications, metal−organic frameworks (MOFs) have stood out due to their inherent designability, which enables rational design of materials with specific pore sizes, topologies, and hydrophilicity. The wide range of structural types has enabled MOFs for use in several applications, including atmospheric water harvesting, heat pumps, desiccation, desalination, humidity control, and thermal batteries.[1,4−7]

Fundamental to many of these applications is the sharp and sudden onset of pore filling at a particular RH. This phenomenon, termed *capillary condensation*, allows for large amounts of water and heat to be cycled over a narrow pressure region. It has been previously demonstrated[8] that the RH for capillary condensation ($\alpha = P/P_{sat}$) can be related to the hydrophilicity of the framework, specifically the difference in Gibbs free energy of water at the pore−framework interface relative to bulk water (ΔG) and the maximum pore radius (r):

$$\ln \frac{P}{P_{sat}} = \frac{2V}{AkT}\frac{\Delta G_{int}}{r} \quad (1)$$

where V is the volume of a molecule of water (calculated from the kinetic diameter), A is the projected interfacial area of a molecule of water, r is the pore radius, k is the Boltzmann constant, T is the temperature, and ΔG_{int} is the difference in Gibbs free energy of water at the interface relative to bulk

Received: February 23, 2024
Revised: July 2, 2024
Accepted: July 3, 2024
Published: July 22, 2024

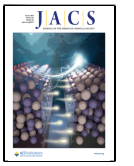

https://doi.org/10.1021/jacs.4c02743
J. Am. Chem. Soc. 2024, 146, 20615−20626

liquid (assuming a cylindrical pore geometry, as most MOF sorbents can be approximated as intersecting cylindrical pores).[8] The pore radius is taken as the radius of the maximally included sphere as capillary condensation is limited by the largest cavity.[9] The prefactor $\frac{2V}{AkT}$ may be approximated assuming a kinetic diameter of water of 2.65 Å and 25 °C, to be $\frac{2V}{AkT} = 1.4 \frac{\text{Å·mol}}{\text{kJ}}$.

Herein, we expand the scope of this relationship by regressing upon 96 MOFs including 32 different chemical group types (as defined by linker backbone, secondary building unit (SBU), and functional group). The regression affords ΔG_{int} values that define a scale for hydrophilicity and enable rational chemical design to affect the RH for capillary condensation. We further derive a scaling relationship between the maximum gravimetric capacity (Q_g) for uptake and maximal pore radius (r), enabling the direct relationship between the critical RH for capillary condensation and the gravimetric capacity for uptake,

$$Q_g = a_1\left(\frac{\Delta G}{\ln \alpha}\right)^2 + a_2\left(\frac{\Delta G}{\ln \alpha}\right) \quad (2)$$

This relationship, which we term *isoreticular curves*, details exactly how the properties for water sorption will respond to an isoreticular expansion of a framework, for a given pore size, topology, and density and volume of framework constituents. The existence and size of hysteretic loops are discussed within the context of isoreticular curves, as capillary condensation hysteresis is intrinsically tied to the maximal pore radius.[10] Additionally, the concept of isoreticular curves gives a basis for discussing the apparent absence of high-capacity sorbents that uptake at low RH (Figure 1). Importantly, for an isoreticular

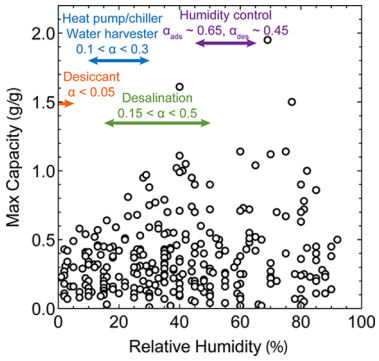

Figure 1. Maximum gravimetric capacity and critical relative humidity for adsorption of water for 276 MOFs. Approximate RH regimes for specific applications are highlighted;[1] we note that these ranges can shift depending on device engineering.

MOF series, simply increasing the pore size (by linker expansion) will cause an increase in the critical RH. The absence of such low RH sorbents is of particular importance for atmospheric water harvesting, as this application requires sorbents that adsorb at low RH.[5] In order to find such sorbents, it is necessary to increase the hydrophilicity of the framework, where the ΔG_{int} scale may be useful.

RESULTS AND DISCUSSION

1. Response of α on Continuous Modulation of Pore Composition. For macroscopic systems, the critical pressure for capillary condensation ($\alpha = P/P_{sat}$) is related to the surface tension and/or contact angle of the fluid on the sorbent as described by the Kelvin or Ostwald–Freundlich equation,

$$\ln \alpha = -\frac{2V}{r_m kT}\gamma \quad (3)$$

where r_m is the curvature radius, V is the molar volume of water, k is the Boltzmann constant, T is the temperature, and γ is the surface tension.[11] This macroscopic theory has been succeeded by microscopic theories, specifically in the case of capillary condensation in slit or cylindrical systems, as described by classical density functional theory.[12,13] These microscopic theories describe the dependence of the critical pressure on the fluid–fluid interaction strength, the wall–fluid interaction strength, and the density distribution of the fluid in the pores. However, even though these equations may be more precise than the macroscopic Kelvin equation, the density functional theory calculations quickly become nonanalytic and still require heavy approximations such as local density treatment of the functional and slab density approximation for the density distribution. As such, even though the precision of the equations may be great, the amount of chemical insight that may be derived from these theories is somewhat limited.

The RH for capillary condensation has also been analyzed with respect to the Henry's law constant, finding that the two have a weak negative correlation to each other. The Henry's constant has been interpreted as a measure for the hydrophilicity of the sorbent at the lowest loading.[2] As such, more hydrophilic frameworks express capillary condensation at lower RH. However, due to the disregard for the effect of pore size, the correlation is weak, and the model predictive power is low.

More recently, the macroscopic Kelvin equation has been extended to microscopic systems, by relating surface tension to the difference in Gibbs free energy between the sorbent–pore interface and bulk liquid (eq 1). Additionally, by assuming that water interacts with framework components independently, the Gibbs free energy, ΔG_{int}, may be decomposed into contributions of each constituent comprising the framework.

Equation 1 operates under a set of underlying assumptions that are somewhat simplistic. The relationship does not account for any nonlinear response of the temperature on the critical chemical potential (e.g., $kT \ln \alpha$ should be slightly temperature dependent below the critical temperature for capillary condensation[12]). The model also does not account for pore wetting; the pore size must be modulated by the thickness of the wetting layer ($r_{eff} = r - t$, where t is the thickness of the wetting film).[14] The assumption that the pore radius can be well-approximated by the largest cavity radius does not fully describe nonuniform pore size distributions, which are very common in MOFs. Finally, the assumption that water interacts with components independently does not fully describe cooperative interactions. However, eq 1 does enable a discussion about how the hydrophilicity of a framework, as defined by its constituents, impacts the RH where capillary condensation occurs. Historically, this has been difficult to probe.

Equation 1 is particularly valuable for the description of sorbents in which the pore environment varies continuously (i.e., solid solutions). For example, for a system with variation between components A and B, with molar fractions x_A and x_B and Gibbs free energies ΔG_A and ΔG_B (assuming that the surface area of components A and B are equal), the average

https://doi.org/10.1021/jacs.4c02743
J. Am. Chem. Soc. 2024, 146, 20615–20626

Gibbs free energy can be expressed as $\Delta G_{int} = x_A \Delta G_A + x_B \Delta G_B$ where $x_A + x_B = 1$. As such,

$$\ln \alpha = \frac{2V}{rAkT}(\Delta G_B + x_A(\Delta G_A - \Delta G_B)) \quad (4)$$

The behavior expressed by eq 4 has been observed in several systems, including continuous variation between MOF-303 and MOF-333, mixed metal (cobalt and zinc) MFU-4l, and variation between MOF-303 and CAU-23, as well as mixed-metal (nickel and zinc) and mixed-anion (chloride and acetate) CFA-1 (Figure 2, Supplemental Section 2).[15−17] In

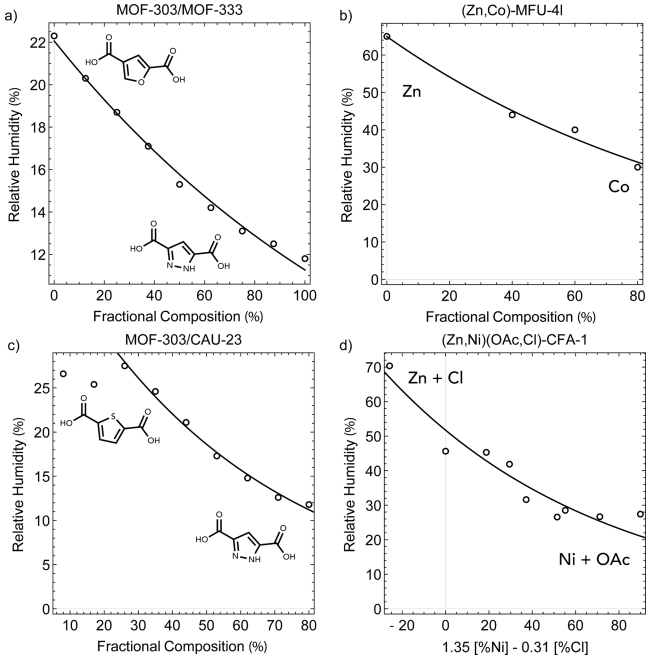

Figure 2. (a) Variation between MOF-303 and MOF-333 (pyrazole and furan dicarboxylate).[15] (b) Variation between Zn-MFU-4l and Co-MFU-4l.[16] (c) Variation between MOF-303 and CAU-23 (pyrazole and thiophene dicarboxylate).[17] (d) Continuous variation of two independent components (reduced to one coordinate).[8]

fact, deviations from the exponential behavior of eq 4 in continuously variable systems may be used to detect structural changes in the respective continuous series. For instance, the dependence of the critical RH on composition for mixed MOF-303 and CAU-23 (Figure 2c) is nonexponential near the CAU-23 limit due to a structural change from an orthorhombic space group with a $(cis)_4$-$(trans)_4$ alternating SBU in CAU-23 to a monoclinic space group with a $(cis)_1$-$(trans)_1$ alternating SBU in MOF-303. Deviations may also arise from cooperative interactions with water. In these cases, a term must be added to the Gibbs free energy relationship, pertaining to the interaction strength of pairs of neighboring components:

$$\Delta G_{int} = x_{AA}\Delta G_{AA} + x_{AB}\Delta G_{AB} + x_{BB}\Delta G_{BB} \quad (5)$$

where $x_{AA} + x_{AB} + x_{BB} = 1$.

2. Regression of α-Pore Composition Dependence on a Curated MOF Data Set. By regressing upon the Gibbs free energy relation (eq 1) using a curated data set of frameworks spanning a wide range of compositional types, an energy scale quantifying the hydrophilicity of frameworks can be determined. Specifically, the regression was performed on 96 frameworks containing 32 compositional types (with a data to parameter ratio of 3) (Table S1). The frameworks were chosen to form a subset of a larger 276 framework data set such that the water isotherms were relatively sharp (i.e., capillary condensation events), had a single uptake step (i.e., single pore type), and the framework was not susceptible to significant structural flexibility (such as that for MIL-53 which presents flexibility induced hysteresis and does not have a constant pore size during sorption[18]). The RH for condensation was taken as the RH at half of maximum capacity (on the adsorption branch, an approximation for the unmeasurable thermodynamic RH in the case of hysteresis), the pore radius was calculated from the maximally included sphere based on the crystal structure, and the prefactor was taken as 1.4 $\frac{\text{Å}\cdot\text{mol}}{\text{kJ}}$. This prefactor may be a source of uncertainty—causing the resultant ΔG values to be off by a scale factor—and could be refined by detailed molecular dynamics simulations.

$$\ln \alpha = \frac{1.4}{r}\Delta G_{int} \quad (6)$$

The functional groups were coarse grained into three categories: SBU type (defined per metal), linker type, and linker functional group type. The ΔG_{int} calculated was averaged by normalizing the energy to the total number of metals and linker types. This normalization takes the approximation that the functional groups do not change the accessible surface areas as significantly as the SBU type and linker type, and that the accessible surface area for each SBU type and linker type is equivalent. This approximation is required as the surface area for each functional group is not known, and there is not enough data to regress an additional parameter for each data point.

$$\Delta G_{int} = \frac{\sum_i^{SBU} n_i \Delta G_i + \sum_i^{linker} n_i \Delta G_i + \sum_i^{func} n_i \Delta G_i}{\sum_i^{SBU} n_i + \sum_i^{linker} n_i} \quad (7)$$

Given that each composition type is not normalized to the exact water accessible surface area, this approximation is potentially a significant source of error for the coarse graining regression. Additionally, each composition type is assumed to be independent, ignoring (un)cooperative interactions between nearest neighbors. The chemical group types were selectively chosen to minimize correlations between composition types (Figure S5). The adjusted R^2 value for the regression is 0.96, with 89% of the data captured within ±10%RH of the experimentally determined α value, and 97% of the data captured within ±20%RH of the experimentally determined α value (Figure 3). The fit values for ΔG_{int} form a hydrophilicity scale for the different composition types (Figure 4). Gratifyingly, even though the regression requires crude approximation and the predicted model only captures the data within ±20% RH, the ordering of this scale qualitatively matches the Gibbs free energy (or logP(water/gas) values) as determined for related molecular species.[19] Given this similarity, it would not be unreasonable to use logP(water/gas) to predict the hydrophilicity of functional groups that have not yet been incorporated into MOFs. We expect that this hydrophilicity scale—and extensions of it derived by higher levels of theory, such as density functional theory[20]—that may be generated in the future, will enable the rational design of frameworks such that the critical RH may be *a priori* determined by modulation of a parent framework with functional groups.

https://doi.org/10.1021/jacs.4c02743
J. Am. Chem. Soc. 2024, 146, 20615−20626

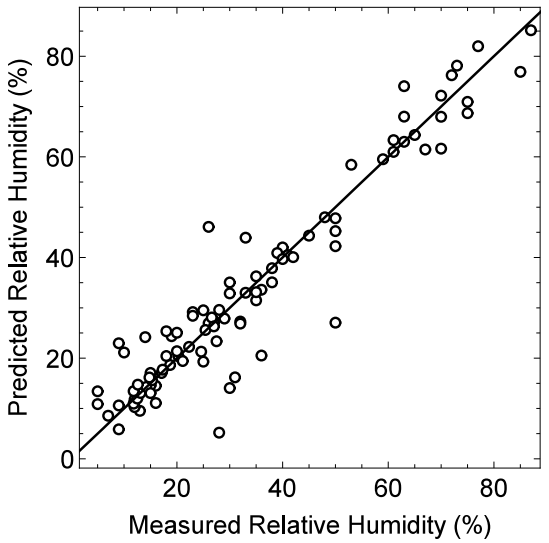

Figure 3. Parity plot of model with dotted lines depicting ±10%RH and ±20%RH deviations.

3. Relationship between Maximum Capacity and Largest Cavity Diameter. One of the most unusual aspects of water sorption using MOFs or covalent organic frameworks (COFs) is the apparent absence of frameworks that have high gravimetric capacity at low RH (gray area in Figures 5 and S7; Tables S3−5). To arrive at an understanding for this phenomenon, it is necessary to understand the relationship between maximum gravimetric capacity, Q_g, and the critical RH for capillary condensation, α. Given that α may be related to the maximal pore radius, by eq 1, a relationship between the Q_g and the maximal pore radius can have the desired effect. Gravimetric capacity is chosen as the measurable parameter, rather than volumetric capacity, as gravimetric capacity is easily and routinely measured for all materials, whereas determination of sample density in order to measure volumetric capacity is not.

It can be shown by a combination of geometric considerations and dimensional analysis that the Q_g scales quadratically with the pore radius, r,

$$Q_g(r) = c_1 r^2 + c_2 r \tag{8}$$

for constants c_1 and c_2 that depend upon framework topology, the volume occupied by the linker and SBU, and the mass of the linker and SBU (Supplemental Section 5). Importantly,

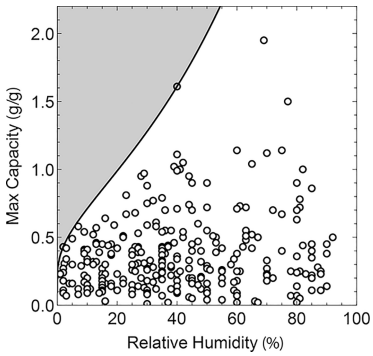

Figure 5. Region of high capacity and low relative humidity that is absent (qualitative low pressure region highlighted according to the equation $Q_{max} = -0.25(1/\ln \alpha)^2 - 1.75(1/\ln \alpha)$, which is valid only in the low relative humidity regime below 60%RH).

this approximation has the boundary condition that Q_g vanishes as the pore radius approaches zero. Ideally, both constants must be positive for Q_g to remain positive for all positive pore radii. However, given the rough approximation that takes only the leading terms in the series approximation, it is often necessary to relax this constraint, and instead restrict the range over which the quadratic dependence is valid.

The quadratic dependence can be empirically observed by inspection of the relationship between the accessible volume and the square of the largest cavity diameter for frameworks of a given topology within a large data set of computed MOF structures (taken from the QMOF database[21,22]). For each topology, the set of frameworks that maximize the accessible volume for a given largest cavity diameter follows a quadratic dependence (Figure 6). The frameworks that lie on this maximally bounding line are the most efficiently packed (i.e., least amount of volume occupied by the linkers and the least dense framework). For example, consider two theoretical MOF structures from the QMOF database with **pcu** topology, qmof-870af3e and qmof-3630fc5. The former is a Zn-pillared paddlewheel structure containing linkages with many alkynyl units, whereas the latter is isoreticular to MOF-5, made from the bulky tetranitroterephthalate (Figure S10). Even though both structures adopt the same topology and have similar largest cavity diameters, 14.03 and 14.16 Å respectively, the large bulk of the tetranitroterepthalate relative to alkynyl units decreases the void fraction from 0.66 to 0.35 and the accessible volume from 1.98 to 0.35 cm^3/g. The Zn-pillared paddlewheel structure may be called *efficiently packed*, as it maximizes the

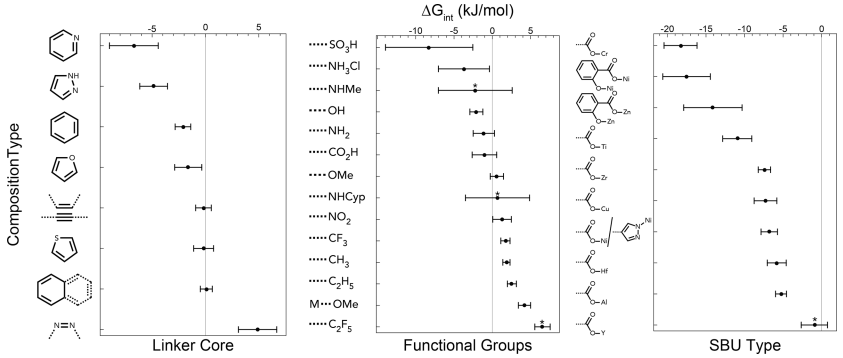

Figure 4. Model determined Gibbs free energy for binding water at the pore water−MOF interface at different composition types. The asterisk indicates composition types that only have one example in the data set.

https://doi.org/10.1021/jacs.4c02743
J. Am. Chem. Soc. 2024, 146, 20615−20626

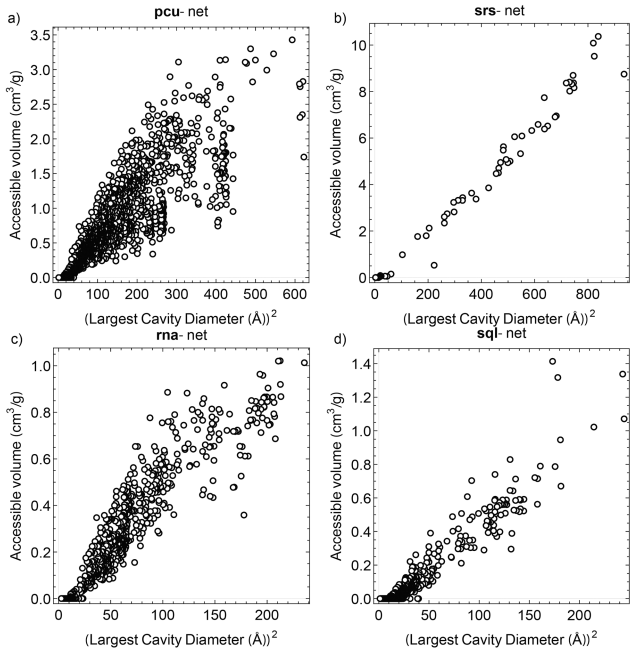

Figure 6. Relationship between the square of the largest cavity diameter and the accessible volume for MOFs in the QMOF database with representative topology **srs**, **pcu**, **rna**, and **sql**. Note that the efficiency front follows a linear dependence between accessible volume and the square of the largest cavity diameter.

accessible volume for a given pore size. The quadratic dependence of the gravimetric capacity can also be observed by calculation of the accessible volume as a function of the radius of the maximally included sphere for the isoreticular series of frameworks, wherein the behavior is well approximated by a quadratic relationship (Supplemental Section 7).

To estimate the dependency of the constants c_1 and c_2 on the topology of a framework, a packing efficiency was calculated for all 3-periodic graphs in the limit of small steric bulk (taken from the RCSR database,[23] Supplemental Section 8). The resulting packing efficiencies dictate a material-independent ordering of topologies that maximizes capacity for a given pore size (and thus maximizes capacity for a given RH). The topologies with the highest packing efficiency that are typically adopted by MOFs are **hex**, **pcu**, **bcu**, **bnn**, and **acs**. One key observation is that topologies with the highest packing efficiencies are those that when projected along the major crystallographic axes result in 2-periodic graphs with high packing efficiency, namely **hxl**, **sql**, **hcb**, and **hgb** (i.e., frameworks with 1-dimensional pores tend to have high packing efficiencies).

4. Relationship between Maximum Capacity and α. Given the relationship between the critical RH for capillary condensation, α, with the largest cavity diameter, $\ln \alpha = \frac{2V}{ArkT}\Delta G_{int}$, and the relationship of the maximum gravimetric capacity with the largest cavity diameter, $Q_g = c_1 r^2 + c_2 r$, the critical RH and gravimetric capacity can be related according to

$$Q_g = a_1\left(\frac{\Delta G}{\ln \alpha}\right)^2 + a_2\left(\frac{\Delta G}{\ln \alpha}\right) \tag{9}$$

where a_1,$a_2 > 0$ are constants that account for the topology, density, and volume occupied of the framework, the size of a molecule of water, and the temperature of the system. Importantly, in the limit as Q_g approaches zero, α vanishes, and in the limit as α approaches 100%, Q_g diverges (i.e., approaches bulk). As mentioned before, in the ideal case a_1,$a_2 > 0$, however due to the many approximations made, this constraint may be allowed to be relaxed and the domain over which the equation is valid may be restricted. If the restrictions on the sign of the constants are relaxed, then the equation will no longer be valid in the large pore limit (as gravimetric capacity may not diverge as the RH approaches unity). The relationship may also be conveniently expressed by

$$Q_g = a_1\left(\frac{1}{\ln \alpha}\right)^2 + a_2\left(\frac{1}{\ln \alpha}\right) \tag{10}$$

wherein the Gibbs free energy is merged into the constants a_1 and a_2, with $a_1 > 0$ and $a_2 < 0$ in the ideal case.

This relationship may be used to understand how modifications to a framework will affect the sorption properties (Figure 7). Upon isoreticular expansion (that preserves the hydrophilicity), both the RH and the maximum capacity will increase. For a modification that increases hydrophilicity, the RH will decrease, and the maximum capacity will remain unchanged. For a modification that increases the packing efficiency (without affecting the pore size or hydrophilicity), there will be an increase in the maximum capacity, but no change to the RH.

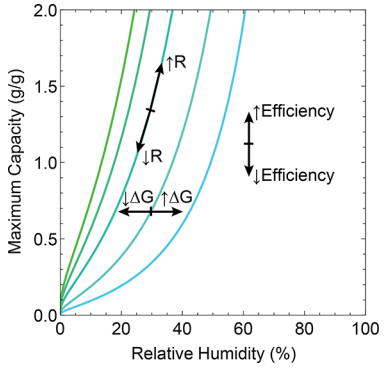

Figure 7. Modulation of an isoreticular curve in response to changes in pore size, hydrophilicity, and packing efficiency.

The gravimetric capacity and RH can be plotted as a series of isoreticular curves. Each isoreticular curve describes a series of isoreticular frameworks with the same hydrophilicity, but different pore sizes. Within the context of the isoreticular curves concept, we propose a quantitative metric describing the most hydrophilic isoreticular curve currently accessible by fitting a maximally bounded isoreticular curve, at

$$Q_g = -0.25\left(\frac{1}{\ln \alpha}\right)^2 - 1.75\left(\frac{1}{\ln\ \alpha}\right) \tag{11}$$

bounding the maximum gravimetric capacity in the low RH regime. This bound may be treated as an analogue to a Robeson limit for membrane separation,[24] as it is not a theoretical limit, but instead the current practical limit. This upper bound relaxes the constraint that $a_1 > 0$ and $a_2 < 0$, as such the range over which it is valid should be limited to below 60%RH.

Importantly, the isoreticular curve concept may be tested against experimental data in which water sorption has been

https://doi.org/10.1021/jacs.4c02743
J. Am. Chem. Soc. 2024, 146, 20615−20626

measured across an isoreticular series of frameworks, such as the $Ni_8L\#$ series or for MCM-41 variants with variable pore size and constant hydrophilicity.[25,26] For both of these series, the relationship between the theoretically calculated accessible volume and the critical RH follows the isoreticular curve well (Figure 8a,b). For the $Ni_8L\#$ series, the isoreticular curve

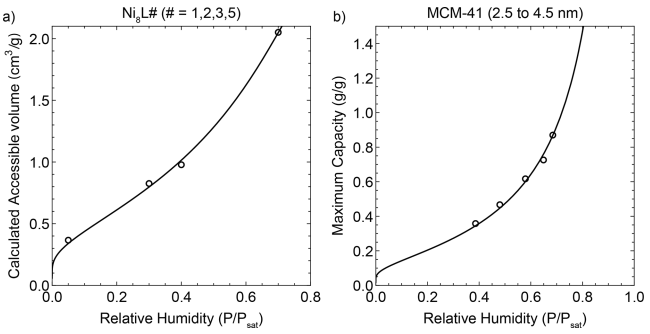

Figure 8. Quadratic fit of $\log[\alpha]$ against calculated accessible volume, $Q_{max} = a_1(1/\ln \alpha)^2 + a_2(1/\ln \alpha)$, (a) for the Ni8L# series where $a_1 = -0.12$ and $a_2 = -1.06$ and (b) for MCM-41 where $a_1 = 0$ and $a_2 = -0.33$.

makes the approximation that the Gibbs free energy for the four frameworks is roughly constant, as each framework uses a slightly different linker (calculated $\Delta G_{int} = -9.1, -11.2, -11.2, -11.5$ kJ/mol, for Ni_8L1, Ni_8L2, Ni_8L3, and Ni_8L5 respectively). Additionally, there is error associated with the determination of the critical RH for each framework in this series as the smaller frameworks have relatively shallow uptake at the point of pore filling, causing uncertainty in the determined value. Given that the composition of the siliceous MCM-41 does not vary upon variation in pore width from 2.5 to 4.5 nm, the Gibbs free energy should be approximately constant. As such, the isoreticular curve (eq 10) can be fit with strict bounds of $a_1 > 0$ and $a_2 < 0$, such that the capacity at saturation vapor pressure diverges. Additionally, the quadratic term vanishes, as a result of there being no SBU unit as well as having purely one-dimensional pores.

4.1. Case Study for Isoreticular Series. Take as example the isoreticular series of aluminum MOFs, with the formula unit Al(OH)(bis-carboxylate), adopting structures approximated by **sql** 2-periodic topologies (Figure 9).[15,17,27−35] Given that these frameworks are anisotropic pores with one-dimensional channels, the highest order term vanishes, and $Q_g = a_1\left(\frac{1}{\ln \alpha}\right)$ is a good approximation of the critical RH dependence of the maximal capacity. Across these frameworks, the identity of the linker and the conformation of the SBU (denoted by the relative position of the hydroxyl groups on the aluminum sites) are varied, affecting the pore size, hydrophilicity, and density of the framework. In this series, many of the all-trans structures, such as MIL-53-BDC, are ignored as they experience a high amount of structural flexibility and the gate opening process affects the thermodynamics of water sorption.

Notably, upon isoreticular expansion (that preserve SBU conformation), such as from MOF-303 (pyrazole dicarboxylic acid) to MOF-321 (vinylpyrazole dicarboxylic acid), MIL-53-fum (fumaric acid) to MIP-211 (muconic acid), or MIL-160 (furan dicarboxylic acid) to MOF-LA2−1(furan) (vinylfuran dicarboxylic acid), the critical RH and maximum capacity tend to move up the isoreticular curves. Isoreticular modification of the chemical constituents without changing the length of the

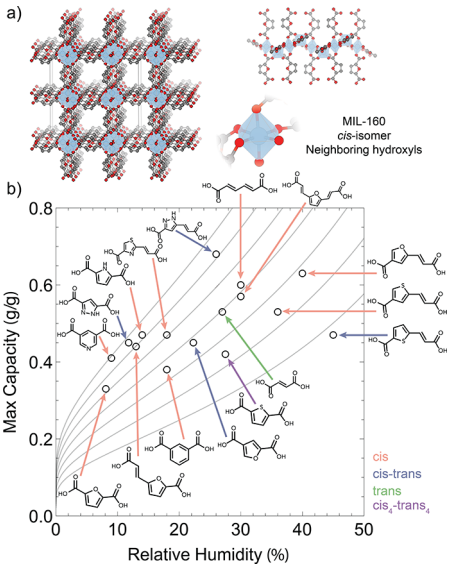

Figure 9. (a) Structure of MIL-160 and depiction of the *cis*-relative orientation of the hydroxyl groups on the aluminum site.[36] (b) Relationship between critical relative humidity and maximum gravimetric capacity for the isoreticular family for aluminum MOFs.

linkers, such as from CAU-10 (benzene dicarboxylic acid) to CAU-10-pydc (pyridine dicarboxylic acid) or MOF-333 (furan dicarboxylic acid) to MOF-303 (pyrazole dicarboxylic acid), tend to decrease the critical RH without significant change to the maximum capacity. Additionally, frameworks with heavy elements, such as CAU-23 (thiophene dicarboxylic acid), have much lower packing efficiencies and lower gravimetric capacities than other frameworks.

When presented together in the maximum capacity−RH phase space, it becomes clear that in order to increase the maximum capacity, while maintaining an RH below 30%, a linker of at least the length of a vinyl-5-membered heterocycle is necessary and the hydrophilicity should be greater than that of vinylpyrazole dicarboxylic acid.

5. Relationship between Largest Cavity Diameter and Hysteresis. The relationship between adsorption−desorption hysteresis and structural properties is less clear-cut than that between structural properties and the critical pressure or maximum gravimetric capacity.[37] This ambiguity often arrives due to the many potential sources of hysteresis, including intrinsic hysteresis due to the metastability of a phase transition,[12] strong wetting or supercluster formation,[38] flexibility or breathing modes,[39] pore blocking due to nonuniform pore distributions,[40] and general sluggish kinetics. Here, we discuss the behavior of intrinsic hysteresis. Typically, this hysteresis is associated with a pore diameter of 20 Å.

Hysteresis induced by capillary condensation is best described by a (pseudo)first-order phase transition between gaseous fluid and condensed fluid. For a first-order phase transition, the size of the hysteretic loop decreases with increasing temperature or with decreasing pore size, with complete disappearance of hysteresis at a critical temperature/critical pore size. However, given that sorbent pores are often quasi-one-dimensional system (*quasi-* indicates that there is finite width to the one-dimensional pores), the transition from gaseous fluid to condensed fluid must be described as a pseudo-first-order phase transition, in which finite size effects cause the appearance of a second critical point, and cause

https://doi.org/10.1021/jacs.4c02743
J. Am. Chem. Soc. 2024, 146, 20615−20626

rounding of the isotherm step.[41] The two critical points are the pore critical point, T_{cp} (denoting the transition from steep to shallow uptake), and the hysteresis critical point, T_{ch} (denoting the transition from hysteresis to no hysteresis). The pore critical point is analogous to the critical point for a first-order phase transition, whereas the hysteresis critical point arises due to the finite size effects (T_{ch} approaches zero as the particle size grows large). Experimentally, T_{ch} is identified by the temperature at which the hysteretic loops vanish, whereas T_{cp} is determined by the temperature at which there is a discontinuity in the slope of the isotherm at the pore filling step as a function of temperature.[42,43]

In the limit where the phase transition is described by a first-order phase transition, the isotherm folds inward onto itself (Figure 10), causing a segment of the path to become unstable

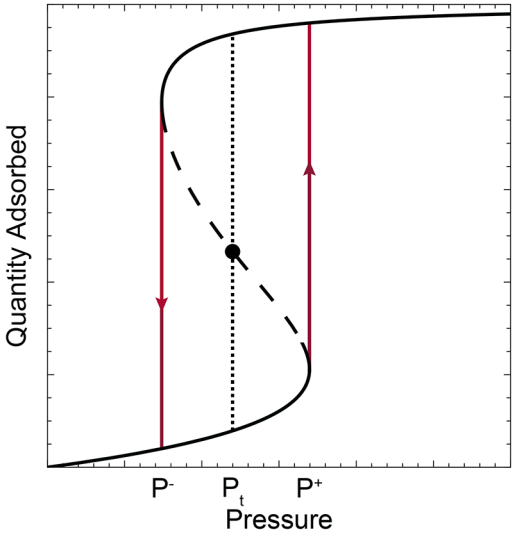

Figure 10. Dependence of the quantity adsorbed on the relative humidity below the critical temperature. The dashed line indicates the underlying equation of state, which is physically inaccessible as the slope is negative. The dotted line represents the thermodynamic pressure at which the phase transition would occur. The red lines indicate the spinodal points at which the phase transition will occur.

(i.e., the region for which $Q_g(P)$ has a negative slope). The equilibrium transition pressure, P_t, is set by the equal area rule.[12,44] During adsorption or desorption, the pressure may go past the equilibrium pressure and the system will be in a metastable state. Given a sufficiently large fluctuation, the system will surmount the barrier for nucleation and undergo the phase transition. It has yet to be demonstrated that particular types of functional groups may be used as points for nucleation. It has also not been demonstrated that external stimuli (such as an external electric field) may be used to generate the necessary fluctuations. At the spinodal decomposition points (indicated by P^- and P^+), any spontaneous fluctuation can cause nucleation of the phase transition.

The dependency between the critical temperature and the critical pore size has been previously studied by use of classical density function theory using the local density approximation and slab density assumption.[12,13] For a slit geometry (i.e., two parallel plates),

$$\frac{T_{cp}^{cap}}{T_c} = 1 - \frac{1 - e^{-\lambda H}}{\lambda H} \tag{12}$$

where T_{cp}^{cap} is the critical temperature for capillary condensation, T_c is the critical temperature of the bulk fluid, λ^{-1} is the length scale for fluid−fluid and fluid-wall interactions, and H is the critical slit width. For a cylindrical geometry,

$$\frac{T_{cp}^{cap}}{T_c} = 1 - 2I_1(\lambda R_c^{cap})K_1(\lambda R_c^{cap}) \tag{13}$$

where I_1 and K_1 are modified Bessel functions and R_c^{cap} is the pore radius.[12,13] These two relationships may be approximated in the limit of large pores as

$$\frac{T_c - T_{cp}^{cap}}{T_c} = \frac{1}{\lambda H} \tag{14}$$

Experimental observations on silicious materials have indicated that this relationship holds,

$$\frac{T_c - T_{cp}^{cap}}{T_c} = \frac{\sigma}{R_c} \tag{15}$$

where σ is the diameter of the fluid and R_c is the pore radius.[9,10,45] Assuming the kinetic diameter for water, at 25 °C the critical pore diameter is 10 Å. It must be noted that these mean field theory relationships are not expected to be accurate for small pore sizes, and the validity of this equation has only been demonstrated for relatively simple fluids in silicates.[10] As such, there is no reason to expect that the critical pore diameter at 25 °C is exactly 10 Å for all materials. However, for MOF-303 (whose largest included sphere diameter is 6.5 Å), the slope of the adsorption step seemingly depends upon temperature above 10 °C, indicating that at 25 °C, the pore critical diameter is greater than 6.5 Å.[46,47]

Whereas T_{cp} is best described by a shifting of the bulk critical temperature due to confinement, T_{ch} is best described by finite size effects.[37,48] The hysteresis critical point has been previously investigated by Ising (lattice gas) models in quasi-one-dimensional systems.[41] Within this model, the critical temperatures are related to the temperatures at which the correlation length scale (i.e., the size of water droplet domains in the pores) are equal to certain physical distances. The pore critical temperature, T_{cp}, is the temperature at which the correlation length is proportional to the pore radius, and the hysteresis critical temperature, T_{ch}, is the temperature at which the correlation length is proportional to the pore length. Below T_{ch}, the correlation length is longer than the particle size, and thus the pore is filled with a single domain (one continuous droplet of water). In the intermediate regime, the correlation length is smaller than the particle size and the pore contains multiple domains accompanied by loss of hysteresis.

For Ising cylinders without any surface fields, the hysteresis critical temperature scales as the cross-sectional area of the pore per the logarithm of the length of the cylinder,

$$T_{ch} \sim \frac{\left(\frac{R}{\sigma}\right)^2}{\log\left(\frac{L}{\sigma}\right)} \tag{16}$$

where σ is the diameter of the fluid, R is the pore radius, and L is the length of the pore. For infinitely long pores, the critical temperature approaches zero, and isotherms will not have hysteretic loops for any finite temperature. The dependence of T_{ch} on pore length has yet to be experimentally verified. However, if the dependence is accurate, then there is

https://doi.org/10.1021/jacs.4c02743
J. Am. Chem. Soc. 2024, 146, 20615−20626

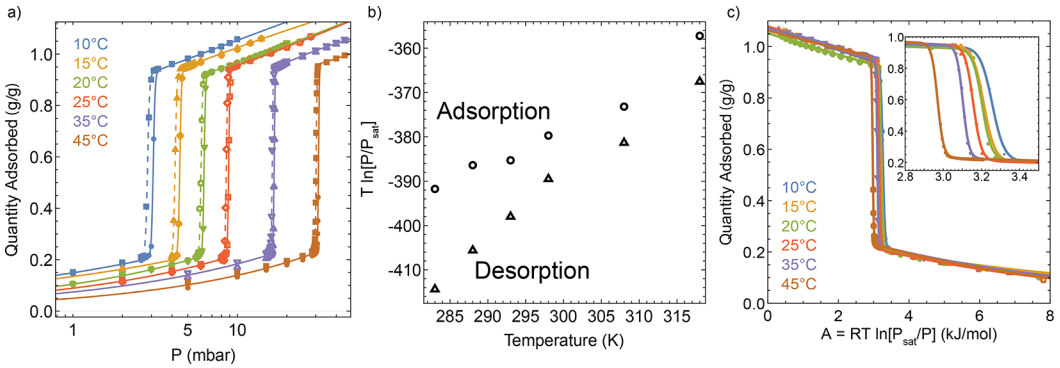

Figure 11. (a) Variable temperature water isotherms of Ni_2Cl_2BTDD (~1 μm long particles). (b) Temperature dependence of adsorption (circle) and desorption (triangle) steps. (c) Characteristic curves for water isotherms of Ni_2Cl_2BTDD at 10, 15, 20, 25, 35, 45 °C.

opportunity for eliminating intrinsic hysteresis in one-dimensional pores of arbitrary pore diameter by increasing particle size. Naturally, this approach is nevertheless likely to induce kinetic limitations to gas uptake when the particle becomes too large.[49]

Analogous to the pore critical point, it has been empirically observed that the following relation for the hysteresis critical point holds:

$$\frac{T_c - T_{ch}^{cap}}{T_c} = \frac{2\sigma}{R_c} \tag{17}$$

where σ is the diameter of the fluid and R_c is the pore radius.[10] Assuming the kinetic diameter for water, at 25 °C the hysteresis pore diameter is 20 Å. Upon examination of the variable temperature water isotherms of Ni_2Cl_2BTDD (rods approximately 1 μm in length as measured by scanning electron microscopy, Figure S17), whose pore size is roughly 20 Å (the largest included sphere diameter is 19 Å and longest Ni−Ni distance in the crystallographic $a-b$ plane is 24 Å), there is a discontinuity in the size of the hysteresis loops at ~25 °C, consistent with the above relationship (Figure 11, Supplemental Section 10). The multidomain behavior of water droplets in the pores of the isoreticular Co_2Cl_2BTDD has been previously observed by molecular dynamics simulations.[50]

As such, it should be expected that above a pore diameter of 10 Å, isotherms should have a sharp uptake and above 20 Å (which may potentially be modified by particle size), isotherms will exhibit adsorption−desorption hysteresis.

6. On Isosteric Enthalpy of Adsorption. Considering that heat transfer during adsorption and desorption is critical for certain applications, accurate measurement of the isosteric enthalpy of adsorption is of particular importance.[51] The isosteric enthalpy (ΔH) is typically calculated by use of the Clausius−Clapeyron relation, which relates the derivative of the logarithm of the pressure with respect to inverse temperature at constant quantity adsorbed, Γ:

$$\left(\frac{\partial \ln P}{\partial\left(\frac{1}{T}\right)}\right)_{\Gamma} = \frac{\Delta H}{R} \tag{18}$$

However, this relation is not necessarily valid for metastable states within a hysteresis loop.[52] More precisely, the apparent enthalpy that is calculated by the Clausius−Clapeyron relation will be composed of the sum of the reversible calorimetric isosteric enthalpy of adsorption, ΔH, and the uncompensated heat for the irreversible isothermal process, Q':[53,54]

$$\left(\frac{\partial \ln P}{\partial\left(\frac{1}{T}\right)}\right)_{\Gamma} = \frac{\Delta H + Q'}{R} \tag{19}$$

In practice, for small hysteretic loops Q' may be much smaller than ΔH, and the apparent isosteric enthalpy may be closely related to the calorimetric heat of adsorption. For large hysteresis loops, such as that observed in Cr-soc-MOF-1,[55] the relative magnitude of Q' relative to ΔH is unknown, implying that the measured isosteric enthalpies may not be accurate. Future studies of water sorption within large-pored frameworks with hysteresis should supplement variable temperature isotherm-derived isosteric enthalpies with calorimetric measurements.

7. On Characteristic Curves. In order to generalize isotherms to arbitrary temperature, water isotherms are often reduced to temperature-invariant characteristic curves by use of the Polanyi equation[56−59]

$$A = RT \ln \frac{P_{sat}}{P} \tag{20}$$

where $\left(\frac{\partial A}{\partial T}\right)_p = 0$. The use of the Polanyi potential assumes that the sorbate behaves as an ideal gas, such that the difference in the chemical potential relative to the standard state follows $\mu - \mu^\circ = RT \ln \frac{P}{P_{sat}}$ for all temperatures. However, the ideal gas assumption is not valid in the case of capillary condensation: the chemical potential of the fluid (at constant partial pressure) is dependent upon temperature (Figure 11b,c, the Polanyi potential for Ni_2Cl_2BTDD is not temperature independent). The Polanyi potential necessarily must be temperature-dependent as the chemical potential of the adsorption branch and desorption branch must coalesce at the hysteresis critical temperature, T_{ch}.[12,45] Over a small temperature range, the Polanyi potential may be approximated as temperature invariant, however approximation will be poor near the critical temperature.

The temperature dependence of the Polanyi potential may be interpreted originating from entropic changes during capillary condensation. Considering the thermodynamic relation $d\mu = -sdT + vdP$, where s is the specific entropy and v is the specific volume. For the case in which the capillary condensation is purely enthalpic, $\left(\frac{\partial \mu}{\partial T}\right)_p = 0$, there is no change in entropy and the chemical potential will be temperature invariant, allowing use of the characteristic

https://doi.org/10.1021/jacs.4c02743
J. Am. Chem. Soc. 2024, 146, 20615−20626

curve. However, in the case in which the capillary condensation involves an entropic change (which should generally be the case during a gaseous-to-liquid phase transition), the chemical potential is temperature dependent, $\left(\frac{\partial \mu}{\partial T}\right)_P = s \neq 0$, and the characteristic curves are not valid.[60]

8. Discussion. It is important to discuss the limitations of the isoreticular curve concept, $Q_g = a_1\left(\frac{\Delta G}{\ln \alpha}\right)^2 + a_2\left(\frac{\Delta G}{\ln \alpha}\right)$ (eq 2) (Figure 12). First, the approximations for the relationship

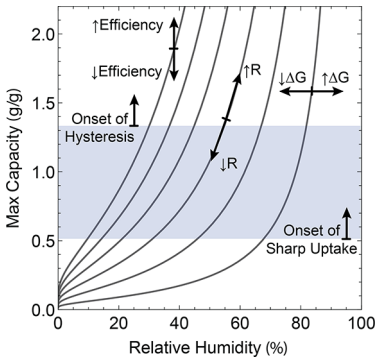

Figure 12. Isoreticular curves that map the maximum capacity-critical relative humidity-intrinsic hysteresis phase space. Isoreticular structural expansion/contractions shift the maximum capacity and critical relative humidity along the isoreticular curves. Expansion above a critical hysteresis pore size (which is framework dependent) triggers hysteresis, and contraction below a critical hysteresis pore size causes uptake to be shallow. The shape of the isoreticular curves and two critical pore sizes depend upon the framework composition, topology, particle size, and temperature.

$\ln \alpha \sim \frac{\Delta G_{int}}{r}$ (eq 1) require that the pore water can be well described by a shell of interfacial water surrounding an interior of pore water. This approximation will break down for pores that are of the same size as the kinetic diameter of water (smaller than the critical pore size for sharp uptake). Additionally, the relationship does not capture pore wetting, which has the effect of reducing the effect pore size. However, as we demonstrate in Section 1, in the pore size regime that is useful for water sorption, these approximations work fairly well. Second, the approximation used for the derivation of the relationship $Q_g(r) = c_1 r^2 + c_2 r$ (eq 8) is that a polynomial fraction can be approximated by a quadratic equation. This approximation will hold if the pore size range that is studied does not vary by more than an order of magnitude. As demonstrated in Supplemental Section 7, this approximation holds over the pore size ranges used for sorption. Taken together, we find that these approximations do not impede description of the relationship between gravimetric capacity and critical RH for the Ni_8L#, MCM-41, and Al(OH)(bis-carboxylate) isoreticular series (as described in Section 4).

Though the key result from the isoreticular curve model is that to increase the maximum capacity of a sorbent, while keeping the critical RH constant, one must increase both the pore size and the hydrophilicity of the framework, the effects of pore hydrophilicity on the kinetics of sorption are not entirely known. It has been previously demonstrated that sorption can occur in various diffusion limited regimes depending upon the geometry of the sorption device. For example, in the case of sorption to a thin layer of MOF, the kinetics of sorption are dictated by the rate of diffusion of gas to the bed of MOF, resulting in rates that are dependent upon the slope of the isotherm.[61] In the case of a thick bed of MOF and fast gas flow, kinetics may instead be dependent upon the intrinsic rate of diffusion of water within the pores of the framework. Recently, it was demonstrated that this rate is dependent upon pore hydrophilicity, and for sufficiently hydrophilic pores, there can be a substantial amount of kinetic hysteresis.[62] A precise relationship between hydrophilicity and diffusion rates has yet to be determined. As such, the regions of the maximum capacity-relative humidity phase space that are useful for practical water sorption (i.e., bounded at high capacity by the onset of intrinsic hysteresis, bounded at low capacity by the low of sharp uptake, and bounded at low RH by kinetic hysteresis; the region contained by the first two are highlighted in Figure 12) may actually be quite small. It is likely that all the state-of-the-art frameworks for water sorption lie in this intermediate regime (Ni_2Cl_2BTDD, MOF-303, CAU-10-H), as they present relatively sharp uptake with minimal hysteretic loops.

There are still several unanswered questions that need to be resolved:

(1) What structural factors dictate cycling stability and how does one design a framework that is indefinitely stable?[63−67] Is cycling stability dependent upon the cycling method (temperature swing or pressure swing, and the rate of temperature or pressure changes)?
(2) What is the effect of dissociative ions on the nature of capillary condensation (such as anilinium chloride or alkali benzenesulfonate functional groups)?[68]
(3) What is the dependence of the enthalpy of adsorption on the pore size and hydrophilicity?
(4) What is a more precise relationship between critical temperature and critical pore radius for confined water (dependent upon pore topology and hydrophilicity)? How does pore wetting affect the two critical points?
(5) Can the capillary condensation phase transition be nucleated closer to the equilibrium chemical potential by perturbation of an external force or by particular types of functional groups?
(6) How much does the apparent isosteric enthalpy of adsorption as calculated by the Clausius−Clapeyron relation differ from the calorimetric heat of adsorption within a large hysteretic loop?

To answer these questions, we hope that the field performs detailed measurements (including both adsorption and desorption isotherms at multiple temperature points), studies the effects of isoreticular modifications to elucidate the underlying principles of sorption, and performs detailed simulations to determine the exact nature of the previously discussed relationships.

There are some additional guidelines for sorbent design that cannot be encompassed within the scope of the model presented by eq 2 but are worth reiterating as they complete the discussion about sorbent design. First, for practical viability, the organic linkers used must be commercially available and inexpensive or have potential routes for cost-effective scale-up. Second, if the intended application is to obtain potable water from the atmosphere, the organic linkers and metals should not be composed of highly toxic materials, to prevent any leaching of hazardous chemicals into the potable water.

https://doi.org/10.1021/jacs.4c02743
J. Am. Chem. Soc. 2024, 146, 20615−20626

CONCLUSION

We propose a relationship between the maximum gravimetric capacity of a sorbent, the hydrophilicity of the pores, and the critical RH for capillary condensation, as described by eq 2. This relationship is derived by the combination of a thermodynamic relationship between critical RH, hydrophilicity (eq 1), and pore size and a geometric relationship between gravimetric capacity and pore size (eq 8). Together, this model enables quantitative design of water sorbents based upon their pore composition and size. Additionally, we discuss the relationship between the two critical points (for onset of sharp uptake, ∼10 Å, and onset of hysteresis, ∼20 Å) and pore size in the context of these other relationships.

We demonstrate the use of eq 1 to construct a quantitative hydrophilicity scale for each component within a sorbent. The resultant hydrophilicity scale correlates well with logP(gas/water) values, implying that literature tabulated values may be used as substitutes to the regressed values.

The factors that contribute to the two variables in eq 2 (a_1 and a_2) depend upon the density and the steric bulk of the components as well as the framework topology. Each topology is ranked according to its packing efficiency, and we find that those containing one-dimensional pores tend to maximize capacity for a given pore size.

Altogether, we find the new design principle for sorbents that maximize gravimetric capacity in the low RH region. Rather than solely increasing pore size to increase capacity (as this will increase the critical RH), the hydrophilicity of the sorbent should be increased, the sorbent should be composed of light elements with a small steric bulk (such as alkynyl units), and the topology should have (pseudo-) one-dimensional pores.

We are just entering the age at which we have full control over the properties for water sorption. The near future will show whether we can tailor materials to have fully desirable properties, capacity, relative humidity, hysteresis, and stability, at affordable costs. We hope that the relationships detailed here will be of use for designing new ultrahigh capacity (>1 g/g) and low or tunable relative humidity frameworks.

ASSOCIATED CONTENT

Supporting Information

The Supporting Information is available free of charge at https://pubs.acs.org/doi/10.1021/jacs.4c02743.

Databases used for modeling, fits used for modeling, Python code to calculate packing efficiency of 3-periodic nets, variable temperature isotherm data and fits for Ni_2Cl_2BTDD (PDF)

AUTHOR INFORMATION

Corresponding Author

Mircea Dincă − *Department of Chemistry, Massachusetts Institute of Technology, Cambridge, Massachusetts 02139, United States*; Email: mdinca@mit.edu

Author

Julius J. Oppenheim − *Department of Chemistry, Massachusetts Institute of Technology, Cambridge, Massachusetts 02139, United States*; orcid.org/0000-0002-5988-0677

Complete contact information is available at: https://pubs.acs.org/10.1021/jacs.4c02743

Author Contributions

All authors have given approval to the final version of the manuscript.

Notes

The authors declare no competing financial interest.

ACKNOWLEDGMENTS

Financial support for this research was generously provided by the Brown Family Foundation through a Brown Investigator Award to M.D. We would like to thank Prof. Francesco Paesani, Dr. Patrick Sarver, Bhavish Dinakar, and Marco Vandone for useful discussions and assistance with scanning electron microscopy.

REFERENCES

(1) Liu, X.; Wang, X.; Kapteijn, F. Water and Metal-Organic Frameworks: From Interaction toward Utilization. *Chem. Rev.* **2020**, *120* (16), 8303−8377.

(2) van der Veen, M. A.; Canossa, S.; Wahiduzzaman, M.; Nenert, G.; Frohlich, D.; Rega, D.; Reinsch, H.; Shupletsov, L.; Markey, K.; De Vos, D. E.; Bonn, M.; Stock, N.; Maurin, G.; Backus, E. H. G. Confined Water Cluster Formation in Water Harvesting by Metal-Organic Frameworks: CAU-10-H versus CAU-10-CH3. *Advanced Materials n/a* **2024**, *36* (12), 2210050.

(3) Xu, Z.-X.; Wang, Y.-M.; Lin, L.-C. Connectivity Analysis of Adsorption Sites in Metal-Organic Frameworks for Facilitated Water Adsorption. *ACS Appl. Mater. Interfaces* **2023**, *15* (40), 47081−47093.

(4) Xu, W.; Yaghi, O. M. Metal-Organic Frameworks for Water Harvesting from Air, Anywhere, Anytime. *ACS Cent. Sci.* **2020**, *6* (8), 1348−1354.

(5) Rao, A. K.; Fix, A. J.; Yang, Y. C.; Warsinger, D. M. Thermodynamic Limits of Atmospheric Water Harvesting. *Energy Environ. Sci.* **2022**, *15* (10), 4025−4037.

(6) Dutta, S.; de Luis, R. F.; Goscianska, J.; Demessence, A.; Ettlinger, R.; Wuttke, S. Metal-Organic Frameworks for Water Desalination. *Adv. Funct. Mater.* **2023***n/a* (n/a), 2304790..

(7) Shi, L.; Kirlikovali, K. O.; Chen, Z.; Farha, O. K. Metal-Organic Frameworks for Water Vapor Adsorption. *Chem.* **2024**, *10*, 484.

(8) Alezi, D.; Oppenheim, J. J.; Sarver, P. J.; Iliescu, A.; Dinakar, B.; Dincă, M. Tunable Low-Relative Humidity and High-Capacity Water Adsorption in a Bibenzotriazole Metal-Organic Framework. *J. Am. Chem. Soc.* **2023**, *145*, 25233.

(9) Coasne, B.; Gubbins, K. E.; Pellenq, R. J.-M. Temperature Effect on Adsorption/Desorption Isotherms for a Simple Fluid Confined within Various Nanopores. *Adsorption* **2005**, *11* (1), 289−294.

(10) Morishige, K.; Ito, M. Capillary Condensation of Nitrogen in MCM-41 and SBA-15. *J. Chem. Phys.* **2002**, *117* (17), 8036−8041.

(11) Gregg, S. J.; Sing, K. S. W. *Adsorption, Surface Area, and Porosity*; Academic Press: London; New York, 1982.

(12) Evans, R.; Marconi, U. M. B.; Tarazona, P. Fluids in Narrow Pores: Adsorption, Capillary Condensation, and Critical Points. *J. Chem. Phys.* **1986**, *84* (4), 2376−2399.

(13) Evans, R.; Marconi, U. M. B.; Tarazona, P. Capillary Condensation and Adsorption in Cylindrical and Slit-like Pores. *J. Chem. Soc., Faraday Trans. 2* **1986**, *82* (10), 1763−1787.

(14) Kruk, M.; Jaroniec, M.; Sayari, A. Application of Large Pore MCM-41 Molecular Sieves To Improve Pore Size Analysis Using Nitrogen Adsorption Measurements. *Langmuir* **1997**, *13* (23), 6267−6273.

(15) Hanikel, N.; Pei, X.; Chheda, S.; Lyu, H.; Jeong, W.; Sauer, J.; Gagliardi, L.; Yaghi, O. M. Evolution of Water Structures in Metal-Organic Frameworks for Improved Atmospheric Water Harvesting. *Science* **2021**, *374* (6566), 454−459.

(16) Wright, A. M.; Rieth, A. J.; Yang, S.; Wang, E. N.; Dinca, M. Precise Control of Pore Hydrophilicity Enabled by Post-Synthetic Cation Exchange in Metal-Organic Frameworks. *Chemical Science* **2018**, *9* (15), 3856−3859.

(17) Zheng, Z.; Hanikel, N.; Lyu, H.; Yaghi, O. M. Broadly Tunable Atmospheric Water Harvesting in Multivariate Metal-Organic Frameworks. *J. Am. Chem. Soc.* **2022**, *144* (49), 22669−22675.
(18) Canivet, J.; Bonnefoy, J.; Daniel, C.; Legrand, A.; Coasne, B.; Farrusseng, D. Structure-Property Relationships of Water Adsorption in Metal-Organic Frameworks. *New J. Chem.* **2014**, *38* (7), 3102−3111.
(19) Duffy, E. M.; Jorgensen, W. L. Prediction of Properties from Simulations: Free Energies of Solvation in Hexadecane, Octanol, and Water. *J. Am. Chem. Soc.* **2000**, *122* (12), 2878−2888.
(20) Keshavarz, F. Dissecting the Water Uptake Behavior of Metal-Organic Frameworks Using Their Isolated Linkers and Metal Nodes. *Chem. Mater.* **2024**, *36*, 439.
(21) Rosen, A. S.; Iyer, S. M.; Ray, D.; Yao, Z.; Aspuru-Guzik, A.; Gagliardi, L.; Notestein, J. M.; Snurr, R. Q. Machine Learning the Quantum-Chemical Properties of Metal-Organic Frameworks for Accelerated Materials Discovery. *Matter* **2021**, *4* (5), 1578−1597.
(22) Rosen, A. S.; Fung, V.; Huck, P.; O'Donnell, C. T.; Horton, M. K.; Truhlar, D. G.; Persson, K. A.; Notestein, J. M.; Snurr, R. Q. High-Throughput Predictions of Metal-Organic Framework Electronic Properties: Theoretical Challenges, Graph Neural Networks, and Data Exploration. *npj Comput. Mater.* **2022**, *8* (1), 1−10.
(23) O'Keeffe, M.; Peskov, M. A.; Ramsden, S. J.; Yaghi, O. M. The Reticular Chemistry Structure Resource (RCSR) Database of, and Symbols for, Crystal Nets. *Acc. Chem. Res.* **2008**, *41* (12), 1782−1789.
(24) Robeson, L. M. The Upper Bound Revisited. *J. Membr. Sci.* **2008**, *320* (1), 390−400.
(25) Padial, N. M.; Quartapelle Procopio, E.; Montoro, C.; López, E.; Oltra, J. E.; Colombo, V.; Maspero, A.; Masciocchi, N.; Galli, S.; Senkovska, I.; Kaskel, S.; Barea, E.; Navarro, J. A. R. Highly Hydrophobic Isoreticular Porous Metal-Organic Frameworks for the Capture of Harmful Volatile Organic Compounds. *Angew. Chem., Int. Ed.* **2013**, *52* (32), 8290−8294.
(26) Jähnert, S.; Chávez, F. V.; Schaumann, G. E.; Schreiber, A.; Schönhoff, M.; Findenegg, G. H. Melting and Freezing of Water in Cylindrical Silica Nanopores. *Phys. Chem. Chem. Phys.* **2008**, *10* (39), 6039−6051.
(27) Zheng, Z.; Alawadhi, A. H.; Chheda, S.; Neumann, S. E.; Rampal, N.; Liu, S.; Nguyen, H. L.; Lin, Y.; Rong, Z.; Siepmann, J. I.; Gagliardi, L.; Anandkumar, A.; Borgs, C.; Chayes, J. T.; Yaghi, O. M. Shaping the Water-Harvesting Behavior of Metal-Organic Frameworks Aided by Fine-Tuned GPT Models. *J. Am. Chem. Soc.* **2023**, *145*, 28284.
(28) Alawadhi, A. H.; Chheda, S.; Stroscio, G. D.; Rong, Z.; Kurandina, D.; Nguyen, H. L.; Rampal, N.; Zheng, Z.; Gagliardi, L.; Yaghi, O. Harvesting Water from Air with High-Capacity, Stable Furan-Based Metal-Organic Frameworks. *ChemRxiv* October 31, **2023**. DOI: 10.26434/chemrxiv-2023-frr55.
(29) Zheng, Z.; Zhang, O.; Nguyen, H. L.; Rampal, N.; Alawadhi, A. H.; Rong, Z.; Head-Gordon, T.; Borgs, C.; Chayes, J. T.; Yaghi, O. M. ChatGPT Research Group for Optimizing the Crystallinity of MOFs and COFs. *ACS Cent. Sci.* **2023**, *9* (11), 2161−2170.
(30) Matemb Ma Ntep, T. J.; Wahiduzzaman, M.; Laurenz, E.; Cornu, I.; Mouchaham, G.; Dovgaliuk, I.; Nandi, S.; Knop, K.; Jansen, C.; Nouar, F.; Florian, P.; Füldner, G.; Maurin, G.; Janiak, C.; Serre, C. When Polymorphism in Metal-Organic Frameworks Enables Water Sorption Profile Tunability for Enhancing Heat Allocation and Water Harvesting Performance. *Adv. Mater.* **2024**, *36* (n/a), 2211302.
(31) Cho, K. H.; Borges, D. D.; Lee, J. S.; Park, J.; Cho, S. J.; Jo, D.; Lee, U.-H.; Maurin, G.; Chang, J.-S. Hydrothermal Green Synthesis of a Robust Al Metal-Organic-Framework Effective for Water Adsorption Heat Allocations. *ACS Sustainable Chem. Eng.* **2022**, *10* (21), 7010−7019.
(32) Hanikel, N.; Kurandina, D.; Chheda, S.; Zheng, Z.; Rong, Z.; Neumann, S. E.; Sauer, J.; Siepmann, J. I.; Gagliardi, L.; Yaghi, O. M. MOF Linker Extension Strategy for Enhanced Atmospheric Water Harvesting. *ACS Cent. Sci.* **2023**, *9* (3), 551−557.
(33) Solovyeva, M.; Krivosheeva, I.; Gordeeva, L.; Aristov, Y. MIL-160 as an Adsorbent for Atmospheric Water Harvesting. *Energies* **2021**, *14* (12), 3586.
(34) Reinsch, H.; van der Veen, M. A.; Gil, B.; Marszalek, B.; Verbiest, T.; de Vos, D.; Stock, N. Structures, Sorption Characteristics, and Nonlinear Optical Properties of a New Series of Highly Stable Aluminum MOFs. *Chem. Mater.* **2013**, *25* (1), 17−26.
(35) Elsayed, E.; AL-Dadah, R.; Mahmoud, S.; Elsayed, A.; Anderson, P. A. Aluminium Fumarate and CPO-27(Ni) MOFs: Characterization and Thermodynamic Analysis for Adsorption Heat Pump Applications. *Applied Thermal Engineering* **2016**, *99*, 802−812.
(36) Wahiduzzaman, M.; Lenzen, D.; Maurin, G.; Stock, N.; Wharmby, M. T. Rietveld Refinement of MIL-160 and Its Structural Flexibility Upon H2O and N2 Adsorption. *Eur. J. Inorg. Chem.* **2018**, *2018* (32), 3626−3632.
(37) Gelb, L. D.; Gubbins, K. E.; Radhakrishnan, R.; Sliwinska-Bartkowiak, M. Phase Separation in Confined Systems. *Rep. Prog. Phys.* **1999**, *62* (12), 1573−1659.
(38) Do, D. D.; Junpirom, S.; Do, H. D. A New Adsorption-Desorption Model for Water Adsorption in Activated Carbon. *Carbon* **2009**, *47* (6), 1466−1473.
(39) Shigematsu, A.; Yamada, T.; Kitagawa, H. Wide Control of Proton Conductivity in Porous Coordination Polymers. *J. Am. Chem. Soc.* **2011**, *133* (7), 2034−2036.
(40) Ball, P. C.; Evans, R. Temperature Dependence of Gas Adsorption on a Mesoporous Solid: Capillary Criticality and Hysteresis. *Langmuir* **1989**, *5* (3), 714−723.
(41) Winkler, A.; Wilms, D.; Virnau, P.; Binder, K. Capillary Condensation in Cylindrical Pores: Monte Carlo Study of the Interplay of Surface and Finite Size Effects. *J. Chem. Phys.* **2010**, *133* (16), 164702.
(42) Morishige, K.; Shikimi, M. Adsorption Hysteresis and Pore Critical Temperature in a Single Cylindrical Pore. *J. Chem. Phys.* **1998**, *108* (18), 7821−7824.
(43) Burgess, C. G. V.; Everett, D. H.; Nuttall, S. Adsorption Hysteresis in Porous Materials. *Pure Appl. Chem.* **1989**, *61* (11), 1845−1852.
(44) Callen, H. B. *Thermodynamics and an Introduction to Thermostatistics*; John Wiley & Sons: 1991.
(45) Morishige, K.; Nakamura, Y. Nature of Adsorption and Desorption Branches in Cylindrical Pores. *Langmuir* **2004**, *20* (11), 4503−4506.
(46) Fathieh, F.; Kalmutzki, M. J.; Kapustin, E. A.; Waller, P. J.; Yang, J.; Yaghi, O. M. Practical Water Production from Desert Air. *Science Advances* **2018**, *4* (6), No. eaat3198.
(47) Hanikel, N.; Prévot, M. S.; Fathieh, F.; Kapustin, E. A.; Lyu, H.; Wang, H.; Diercks, N. J.; Glover, T. G.; Yaghi, O. M. Rapid Cycling and Exceptional Yield in a Metal-Organic Framework Water Harvester. *ACS Cent. Sci.* **2019**, *5* (10), 1699−1706.
(48) Monson, P. A. Understanding Adsorption/Desorption Hysteresis for Fluids in Mesoporous Materials Using Simple Molecular Models and Classical Density Functional Theory. *Microporous Mesoporous Mater.* **2012**, *160*, 47−66.
(49) Colwell, K. A.; Jackson, M. N.; Torres-Gavosto, R. M.; Jawahery, S.; Vlaisavljevich, B.; Falkowski, J. M.; Smit, B.; Weston, S. C.; Long, J. R. Buffered Coordination Modulation as a Means of Controlling Crystal Morphology and Molecular Diffusion in an Anisotropic Metal-Organic Framework. *J. Am. Chem. Soc.* **2021**, *143* (13), 5044−5052.
(50) Zaragoza, A.; Factorovich, M.; Molinero, V. Multi-Stage Condensation Pathway Minimizes Hysteresis in Water Harvesting with Large-Pore Metal-Organic Frameworks. *ChemRxiv* August 21, 2023. DOI: 10.26434/chemrxiv-2022-06264-v2.
(51) Nuhnen, A.; Janiak, C. A Practical Guide to Calculate the Isosteric Heat/Enthalpy of Adsorption via Adsorption Isotherms in Metal-Organic Frameworks, MOFs. *Dalton Transactions* **2020**, *49* (30), 10295−10307.

(52) Hill, T. L. Statistical Mechanics of Adsorption. V. Thermodynamics and Heat of Adsorption. *J. Chem. Phys.* **1949**, *17* (6), 520−535.
(53) La Mer, V. K. The Calculation of Thermodynamic Quantities from Hysteresis Data. *J. Colloid Interface Sci.* **1967**, *23* (2), 297−301.
(54) Everett, D. H.; Whitton, W. I.; Garner, W. E. A Thermodynamic Study of the Adsorption of Benzene Vapour by Active Charcoals. *Proceedings of the Royal Society of London. Series A. Mathematical and Physical Sciences* **1955**, *230* (1180), 91−110.
(55) Towsif Abtab, S. M.; Alezi, D.; Bhatt, P. M.; Shkurenko, A.; Belmabkhout, Y.; Aggarwal, H.; Weseliński, Ł. J.; Alsadun, N.; Samin, U.; Hedhili, M. N.; Eddaoudi, M. Reticular Chemistry in Action: A Hydrolytically Stable MOF Capturing Twice Its Weight in Adsorbed Water. *Chem.* **2018**, *4* (1), 94−105.
(56) Rieth, A. J.; Wright, A. M.; Skorupskii, G.; Mancuso, J. L.; Hendon, C. H.; Dincă, M. Record-Setting Sorbents for Reversible Water Uptake by Systematic Anion Exchanges in Metal-Organic Frameworks. *J. Am. Chem. Soc.* **2019**, *141* (35), 13858−13866.
(57) de Lange, M. F.; van Velzen, B. L.; Ottevanger, C. P.; Verouden, K. J. F. M.; Lin, L.-C.; Vlugt, T. J. H.; Gascon, J.; Kapteijn, F. Metal-Organic Frameworks in Adsorption-Driven Heat Pumps: The Potential of Alcohols as Working Fluids. *Langmuir* **2015**, *31* (46), 12783−12796.
(58) Polanyi, M. Section III.—Theories of the Adsorption of Gases. A General Survey and Some Additional Remarks. Introductory Paper to Section III. *Trans. Faraday Soc.* **1932**, *28* (0), 316−333.
(59) Dubinin, M. M. Physical Adsorption of Gases and Vapors in Micropores. In *Progress in Surface and Membrane Science*; Cadenhead, D. A., Danielli, J. F., Rosenberg, M. D., Eds.; Elsevier: 1975; Vol. *9*, pp 1−70. DOI: 10.1016/B978-0-12-571809-7.50006-1.
(60) Shimizu, S.; Matubayasi, N. Temperature Dependence of Sorption. *Langmuir* **2021**, *37* (37), 11008−11017.
(61) Bezrukov, A. A.; O'Hearn, D. J.; Gascón-Pérez, V.; Darwish, S.; Kumar, A.; Sanda, S.; Kumar, N.; Francis, K.; Zaworotko, M. J. Metal-Organic Frameworks as Regeneration Optimized Sorbents for Atmospheric Water Harvesting. *Cell Reports Physical Science* **2023**, *4* (2), 101252.
(62) Oppenheim, J. J.; Ho, C.-H.; Alezi, D.; Andrews, J. L.; Chen, T.; Dinakar, B.; Paesani, F.; Dincă, M. Cooperative Interactions with Water Drive Hysteresis in a Hydrophilic Metal-Organic Framework. *Chem. Mater.* **2024**, *36* (7), 3395−3404.
(63) Wang, K.; Li, Y.; Xie, L.-H.; Li, X.; Li, J.-R. Construction and Application of Base-Stable MOFs: A Critical Review. *Chem. Soc. Rev.* **2022**, *51* (15), 6417−6441.
(64) Rieth, A. J.; Wright, A. M.; Dincă, M. Kinetic Stability of Metal-Organic Frameworks for Corrosive and Coordinating Gas Capture. *Nat. Rev. Mater.* **2019**, *4* (11), 708−725.
(65) Wang, Z.; Bilegsaikhan, A.; Jerozal, R. T.; Pitt, T. A.; Milner, P. J. Evaluating the Robustness of Metal-Organic Frameworks for Synthetic Chemistry. *ACS Appl. Mater. Interfaces* **2021**, *13* (15), 17517−17531.
(66) Nandy, A.; Duan, C.; Kulik, H. J. Using Machine Learning and Data Mining to Leverage Community Knowledge for the Engineering of Stable Metal-Organic Frameworks. *J. Am. Chem. Soc.* **2021**, *143* (42), 17535−17547.
(67) Liu, J.; Prelesnik, J. L.; Patel, R.; Kramar, B. V.; Wang, R.; Malliakas, C. D.; Chen, L. X.; Siepmann, J. I.; Hupp, J. T. A Nanocavitation Approach to Understanding Water Capture, Water Release, and Framework Physical Stability in Hierarchically Porous MOFs. *J. Am. Chem. Soc.* **2023**, *145*, 27975.
(68) An, H. J.; Sarker, M.; Yoo, D. K.; Jhung, S. H. Water Adsorption/Desorption over Metal-Organic Frameworks with Ammonium Group for Possible Application in Adsorption Heat Transformation. *Chemical Engineering Journal* **2019**, *373*, 1064−1071.

https://doi.org/10.1021/jacs.4c02743
J. Am. Chem. Soc. 2024, 146, 20615−20626